

### Insight into the Effect of Surface Carboxyl and Amino Groups on the Adsorption of Titanium Dioxide for Acid Red G

Journal:	<i>Frontiers of Chemical Science and Engineering</i>
Manuscript ID	FCSE-2020-0167.R1
Manuscript Type:	Research Article
Date Submitted by the Author:	21-Jun-2020
Complete List of Authors:	Zhang, Wenlong; Xi'an Jiaotong University Zhao, Xuyang; Xi'an Jiaotong University Zhang, Lin; Xi'an Jiaotong University Zhu, Jinwei; Xi'an Jiaotong University; Shaanxi Electrical Equipment Institution Li, Shanshan; Xi'an Jiaotong University Hu, Ping; Shaanxi Polytechnic Institute Feng, Jiangtao; Xi'an Jiaotong University, Yan, Wei ; Xi'an Jiaotong University
Keywords:	Amino group, Carboxylic group, Titanium dioxide, Acid Red G (ARG), Adsorption
Speciality Area:	Separation science and technology, Functional material

SCHOLARONE™  
Manuscripts

# Insight into the Effect of Surface Carboxyl and Amino Groups on the Adsorption of Titanium Dioxide for Acid Red G

Wenlong Zhang<sup>1</sup>, Xuyang Zhao<sup>1</sup>, Lin Zhang<sup>1</sup>, Jinwei Zhu<sup>1, 2</sup>, Shanshan Li<sup>1</sup>, Ping Hu<sup>3</sup>,  
Jiangtao Feng<sup>1\*</sup>, Wei Yan<sup>1</sup>

<sup>1</sup>Department of Environmental Science and Engineering, Xi'an Jiaotong University,  
Xi'an 710049, P.R. China

<sup>2</sup>Shaanxi Electrical Equipment Institution, Xi'an 710025, P.R. China

<sup>3</sup>Shaanxi Polytechnic Institute, Xianyang, 712000, Shaanxi, P.R. China

**Abstract:** In this study, Titanium dioxide (TiO<sub>2</sub>) functionalized with organic groups were prepared to study the effect of carboxyl and amino groups on the adsorption behavior of TiO<sub>2</sub> for the removal of Acid Red G (ARG) as an anionic dye from aqueous solution. TiO<sub>2</sub> was successfully modified with carboxyl and amino groups by using the hydrolysis method with oxalic acid (OAD, with two carboxyl groups), ethylenediamine (EDA, with two amino groups) and DL-alanine (DLA, with one carboxyl group and one amino group) at low temperature (65°C) and labeled as OAD-TiO<sub>2</sub>, EDA-TiO<sub>2</sub> and DLA-TiO<sub>2</sub>, respectively. The ARG uptake by the functionalized TiO<sub>2</sub> samples was largely dependent on the functional groups. The interaction between ARG and the functional organic groups on the TiO<sub>2</sub> samples plays an important role in the adsorption process, which leads to the excellent adsorption performance (higher capacity and faster adsorption rate) of the functionalized TiO<sub>2</sub> samples than that of P25 (commercial TiO<sub>2</sub>

---

\* Corresponding Author.

E-mail address: [fjtes@xjtu.edu.cn](mailto:fjtes@xjtu.edu.cn) (J.T. Feng)

without modification). Furthermore, there is no obvious loss of the adsorption capacity for the functionalized TiO<sub>2</sub> even after 5 adsorption-desorption cycles, which indicated the good reusability of the modified TiO<sub>2</sub> samples for anionic dye removal from aqueous solution.

**Keywords:** Amino group, Carboxylic group, Titanium dioxide, ARG, Adsorption

## 1. Introduction

Titanium dioxide (TiO<sub>2</sub>) is a remarkable photocatalyst and numerous researches about heterogeneous photocatalysis related to TiO<sub>2</sub> have been published [1-4]. Due to the excellent photochemical property, TiO<sub>2</sub> is also employed as a catalyst for the pollution removal from air or water [5-7]. Moreover, the adsorption ability of TiO<sub>2</sub> plays an important role in the effective photo degradation of organic matters, although TiO<sub>2</sub> is usually used as the photocatalyst [8].

The pristine TiO<sub>2</sub> has a limited adsorption capacity due to its intrinsic defects, such as low specific surface area and few surface active sites [9]. Meanwhile, the surface active sites are considered to be one of the most significant factors for the adsorption process [10]. Nowadays, an increasing number of studies focused on the approaches to enhance the adsorption property of TiO<sub>2</sub>. Introducing the functional groups onto the TiO<sub>2</sub> surface, such as hydroxyl, carboxyl or amino groups, has been considered as one of the effective methods. In addition, the functional groups bring TiO<sub>2</sub> not only the enhanced adsorption capacity, but also an increased adsorption rate [11].

The introduction of hydroxyl, carboxyl or amino groups can change the surface charge and electron distribution of TiO<sub>2</sub> and influence the interactions between the

adsorbates and the modified TiO<sub>2</sub>. Therefore, the enhanced adsorption capacity of TiO<sub>2</sub> for organic and inorganic adsorbates could probably be achieved by the functionalization of the hydroxyl, carboxyl or amino groups [12, 13]. It was reported that the carboxyl modification could be in favor of the cations adsorption [12]. On the contrary, the amino functionalization was propitious to the adsorption of the anions contaminants [13].

The surface functional groups like carboxyl and amino were usually introduced onto TiO<sub>2</sub> by two approaches. One is anchoring the relevant organic groups onto the surface of the as-prepared TiO<sub>2</sub> particles [14]. In this method, the modified TiO<sub>2</sub> was obtained at higher temperature to strengthen the binding force between the functional groups and TiO<sub>2</sub> structure. The other way is the in-situ synthesis [15], which is a reaction of titanium source (usually tetrabutyl titanate, isopropyl titanate or titanium chloride) and chemicals containing functional groups [16]. The preferable functionalized TiO<sub>2</sub> is obtained by the latter facile method in one step hydrothermal process at lower temperature.

The carboxyl groups can be linked to TiO<sub>2</sub> with the bond formation of bridging, chelating and ester-like linkage [17, 18]. Lee et al [15] found that the carboxylate groups of succinic acid could be coordinated to TiO<sub>2</sub> in the form of bridging and chelating structure after calcined at 400°C for 5 h. The maximum capacity of the modified TiO<sub>2</sub> for methylene blue (MB) was reported as 32.15 mg/g. The amino groups could be grafted on TiO<sub>2</sub> by the hydrogen bonding between NH<sub>2</sub> group and hydroxyl or carboxyl group on TiO<sub>2</sub> surface [19, 20]. For instance, Masanobu Mori et al [13] synthesized an

amino functionalized  $\text{TiO}_2$  with 3-[2-(2-aminoethylamino) ethylamino] propyl-trimethoxysilane (DETA) and the modified sample exhibited more excellent adsorption capacity for indigo carmine than that of pristine  $\text{TiO}_2$ .

Based on the above discussions, we focus on the influence of carboxyl and amino groups on adsorption performance of  $\text{TiO}_2$ . The  $\text{TiO}_2$  samples modified by the organic chemicals with carboxyl and/or amino groups were prepared at low temperature. ARG, one of the typical anionic dyes in wastewater which could cause severe pollution[21], was employed as the target contaminant to examine the effect of functional groups in the adsorption process. It is found that the carboxyl and amino functionalization significantly affect the adsorption behavior of the  $\text{TiO}_2$  samples for anionic dye ARG.

## 2. Experimental

### 2.1. Materials

Tetrabutyl titanate (TBT, 340.36 g/mol, 98%), n-propanol(60.10 g/mol, 99%), oxalic acid (OAD, 90.04 g/mol, 99.5%), ethylenediamine (EDA, 60.10 g/mol, 99.0%) and DL-alanine (DLA, 89.09 g/mol, 98.5%) were of analytical grade and got from Sinopharm Chemical Reagent Co., Ltd., Shanghai, China. Anionic dye ARG (509.42 g/mol, 99.0%) was purchased from Beijing Chemical Reagent Co. of China and used as received. The deionized water used in this study was obtained from the EPED-40TF Superpure Water System (EPED, China).

### 2.2. Synthesis of functional $\text{TiO}_2$ samples

The functional  $\text{TiO}_2$  samples were prepared by the one-step hydrolysis approach at a low temperature. A typical pathway was as follows: firstly, the organic compound

(OAD, EDA or DLA) was dissolved into deionized water to form the 0.16 mol/L solution which was labeled as solution A. The mixture solution containing TBT and n-propanol (the volume ratio is 5:2) was also prepared and named solution B. Then, 14 mL solution B was slowly added into 200 mL solution A with magnetic stirring (300 rpm) for 2 h at 65°C, the white suspension solution was formed. And the suspension was stirred for another 12 h at the ambient temperature. After that, the white solid was collected by filtration and rinsed with water until the pH value of the filtrate was neutral. The collected white solid was dried at 60°C for 24 h. the as-prepared samples were labeled as OAD-TiO<sub>2</sub>, EDA-TiO<sub>2</sub> or DLA-TiO<sub>2</sub> according to the organic compound added in the preparation process. The P25 from the Degussa was employed as the non-functional group comparator.

### 2.3. Analysis and characterization methods

Fourier Transform Infrared spectra (FT-IR) of the samples were carried out on BRUKER TENSOR 37 FT-IR spectrophotometer in the range of 4000-400 cm<sup>-1</sup> by the KBr pellet method. The morphology and elemental information were obtained on a scanning electron microscopy (SEM, JSM-6700F, Japan) with an energy dispersive X-ray spectroscopy (EDX). The thermogravimetric analysis (TG) was performed on a Setaram Labsys Evo in N<sub>2</sub> flow with the heating rate of 10°C/min over a temperature within 30-800°C. Zeta potentials were tested with NanoBrook 90Plus Analyzer. Samples for zeta potential measurement were prepared by adding 1 mg of TiO<sub>2</sub> into 10 mL NaCl solution (0.1 mmol/L) at different pH values from 2 to 12 (adjusted with 0.1 mol/L HNO<sub>3</sub> or NaOH solution). N<sub>2</sub> adsorption and desorption isotherms were recorded

on a Builder SSA-4200 at 77K. The specific surface area is calculated using the multiple point BET method, and total pore volume and average pore radius were calculated based on the BJH (Barrett-Joyner-Halenda) method (using the desorption branch).

## 2.4. Adsorption experiments

The adsorption of ARG was carried out by shaking the mixture of solution with the modified TiO<sub>2</sub> samples (2.0 g/L) at 25°C. Then the suspension was centrifuged at 4000 rpm for 5 min. The supernatant was analyzed by the UV-Vis spectrophotometer (Agilent 8453) and the absorbance value was read at the wavelength of 531 nm, in order to evaluate the adsorption capacity of ARG onto TiO<sub>2</sub> samples.

The amount of ARG molecules adsorbed onto the TiO<sub>2</sub> samples  $Q_t$  (mg/g) at a certain time  $t$  was calculated from Eq. (1):

$$Q_t = \frac{C_0 - C_t}{m} \times V \quad (1)$$

where  $C_0$  (mg/L) and  $C_t$  (mg/L) are the initial concentration and residual concentration at time  $t$  (min) of the ARG solution, respectively;  $V$  (L) is the ARG solution volume, and  $m$  (g) is TiO<sub>2</sub> sample mass.

Adsorption kinetic experiments were carried out in a conical flask by contacting 0.1 g of the TiO<sub>2</sub> samples and 50 mL solution with certain concentration (100, 200, 300 mg/L in this study) of ARG solution at 25°C. In various contact time from 0 to 120 min, 2 mL samples were withdrawn and filtered to evaluate the adsorption capacity of the TiO<sub>2</sub> samples. The Pseudo-first order and Pseudo-second order models (please see Eqs. (2) and (3)) were employed to fit the kinetic experiment data.

$$Q_t = Q_e (1 - e^{-K_1 t}) \quad (2)$$

$$Q_t = \frac{K_2 Q_e^2 t}{1 + K_2 Q_e t} \quad (3)$$

where  $t$  is the adsorption time (min);  $K_1$  ( $\text{min}^{-1}$ ) and  $K_2$  ( $\text{g}/(\text{mg} \cdot \text{min})$ ) are the rate constants for the pseudo-first-order and pseudo-second-order models, respectively;  $Q_t$  and  $Q_e$  ( $\text{mg/g}$ ) are the adsorption capacity at  $t$  min and equilibrium time, respectively. The adsorption isotherms of ARG onto the  $\text{TiO}_2$  samples were obtained by mixing different initial concentrations (10-500  $\text{mg/L}$ ) of ARG solution with 2  $\text{g/L}$  of the  $\text{TiO}_2$  samples, and then the solution was shaken for 120 min in dark at  $25^\circ\text{C}$ . The Langmuir and Freundlich isotherm models were described according to Eqs. (4) and (5), respectively:

$$Q_t = \frac{Q_{\max} K_L C_t}{1 + K_L C_t} \quad (4)$$

$$Q_e = K_F C_e^{1/n} \quad (5)$$

where  $Q_{\max}$  ( $\text{mg/g}$ ) is the maximum monolayer molecular adsorption capacity onto the adsorbent in Langmuir isotherm model;  $K_L$  ( $\text{L/mg}$ ) and  $K_F$  ( $(\text{mg/g})/(\text{mg/L})^n$ ) are the constant of Langmuir and Freundlich isotherm model, respectively.  $1/n$  represents the degree of adsorption dependence on equilibrium concentration in Freundlich isotherm model.

In addition, the dimensionless separation factor  $R_L$ , an essential characteristic of the Langmuir model to reflect the favorability of an adsorption process, is expressed as:

$$R_L = \frac{1}{1 + K_L C_m} \quad (6)$$

where  $C_m$  ( $\text{mg/L}$ ) is the maximum initial concentration of ARG in solution.



In the regeneration study, 200 mg/L ARG solution was being contacted with the  $\text{TiO}_2$  sample for 120 min. Then, the exhausted  $\text{TiO}_2$  sample was immersed in 0.1 mol/L NaOH solution for 20 min to release ARG from the  $\text{TiO}_2$  sample, and further immersed in 0.1 mol/L  $\text{HNO}_3$  solution to activate. The regenerated  $\text{TiO}_2$  sample was again used as the adsorbent to remove ARG from the aqueous solution. And the adsorption capacity of the regenerated  $\text{TiO}_2$  was recorded to evaluate the regeneration property of the functional  $\text{TiO}_2$  samples and P25.

### 3. Results and Discussion

#### 3.1. Characterizations of $\text{TiO}_2$ samples

The FT-IR spectra (please see Fig. 1) of P25 and the modified  $\text{TiO}_2$  samples were analyzed to examine the existence of the functional groups. For P25, the wide peak between 900-400  $\text{cm}^{-1}$  belongs to the Ti-O-Ti stretching vibration [22]. The other wide peak at 3600-3200  $\text{cm}^{-1}$  is very weak and ascribed to the stretch of hydroxyl groups on the surface of  $\text{TiO}_2$  (P25). The peaks for the copious groups in the functionalized  $\text{TiO}_2$  samples appear in the FT-IR spectra. The broad peak in the range of 3600-2500  $\text{cm}^{-1}$  is attributed to the vibration of -OH in carboxylic group. The peaks for - $\text{NH}_2$  stretching vibration (3450-3220  $\text{cm}^{-1}$ ) and strong peak of -OH group are overlapped in this broad range of the spectra of EDA- $\text{TiO}_2$  and DLA- $\text{TiO}_2$ . A broad and strong peak at 1690  $\text{cm}^{-1}$  in the spectrum of OAD- $\text{TiO}_2$  is ascribed to the C=O stretching vibration of saturated dicarboxylic acid. The peaks at 1620 and 1430  $\text{cm}^{-1}$  are related to the asymmetric and symmetric bending vibrations of  $\text{COO}^-$  group, respectively. The value of  $\Delta\nu(\text{COO}^-)$  for the OAD- $\text{TiO}_2$  sample is approximate 190  $\text{cm}^{-1}$ , which illustrates a

bridging structure between OAD and  $\text{TiO}_2$  [23-25]. The peak at  $1288\text{ cm}^{-1}$  corresponds to the stretching vibration of C-O bond. While for the EDA- $\text{TiO}_2$  and DLA- $\text{TiO}_2$  samples, N-H bending vibration of primary amine are observed at around  $1620\text{ cm}^{-1}$ . The peak at  $1510\text{ cm}^{-1}$  (only for EDA- $\text{TiO}_2$ , which is not found in the spectrum of DLA- $\text{TiO}_2$ ) is ascribed to the deformation vibration of N-H in the secondary amine, which indicates there is hydrogen bonding between the amino group and  $\text{TiO}_2$  [19]. The bond at  $1326\text{ cm}^{-1}$  (for EDA- $\text{TiO}_2$ ) is assigned to the stretching vibration of C-N [26]. At the spectrum of DLA- $\text{TiO}_2$ , the peak belonging to C=O disappears, which might be caused by the binding of the carboxyl in the DLA and the  $\text{TiO}_2$  with chelation [23]. The analysis of FT-IR results demonstrates the existence of carboxyl and amino groups and success of  $\text{TiO}_2$  functionalization.

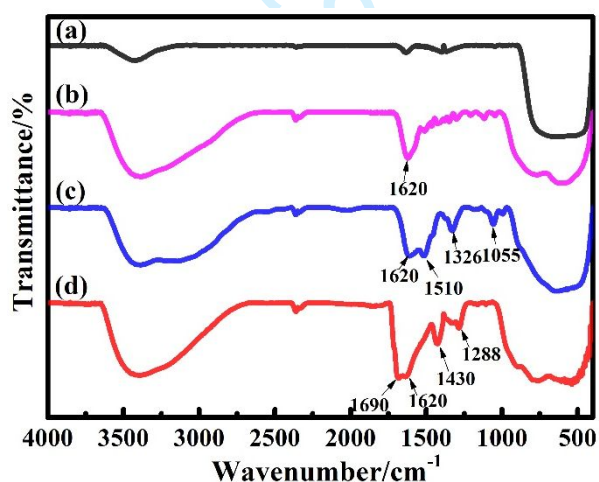


Figure 1. FT-IR spectra of (a) P25, (b) DLA- $\text{TiO}_2$ , (c) EDA- $\text{TiO}_2$  and (d) OAD- $\text{TiO}_2$ .

The morphologies of the  $\text{TiO}_2$  samples are observed by SEM (Fig. S1 with EDX results). The particle size of P25 is so small that the image is not so clear even the magnification is 10000 times. The functional  $\text{TiO}_2$  samples are composed of the micro-particles. And the particle size of OAD- $\text{TiO}_2$  is significantly larger than that of EDA-

TiO<sub>2</sub> and DLA-TiO<sub>2</sub>. In addition, it is obvious that there are certain amounts of pore existing in the structure of EDA-TiO<sub>2</sub> and DLA-TiO<sub>2</sub>. These results suggested that the difference of amino acid used in functional synthesis could cause effect on the morphology of the prepared materials. Furthermore, the group species and number contained in amino acid might be the main factor and amino groups are probably more beneficial to the porous and granular morphology than carboxy groups.

The surface content of each element was also obtained by EDX and listed in Table 1. The functionalization degree may be described by the atom molar C/Ti because C is primarily associated with organic matter in the samples. The C/Ti ratio for the functional TiO<sub>2</sub> samples (C/Ti=0.137, 0.207 and 0.547 for OAD-TiO<sub>2</sub>, EDA-TiO<sub>2</sub> and DLA-TiO<sub>2</sub> respectively) was much higher than that of P25 (C/Ti=0.065), which suggests that these samples contain a great amount of organic residues. The above result indicates certain original organic structures were successfully introduced to these functional TiO<sub>2</sub>, which is consistent with the results of FT-IR spectra.

Table 1. The surface molar ratio of different atoms for the TiO<sub>2</sub> samples.

Sample	C/atom%	Ti/ atom %	O/ atom %	C/Ti
P25 <sup>a)</sup>	4.19	63.69	32.12	0.065
OAD-TiO <sub>2</sub> <sup>b)</sup>	8.18	59.90	28.57	0.137
EDA-TiO <sub>2</sub> <sup>c)</sup>	11.93	57.61	30.47	0.207
DLA-TiO <sub>2</sub> <sup>d)</sup>	24.68	45.09	30.23	0.547

a) P25: commercial bare TiO<sub>2</sub>; b) OAD-TiO<sub>2</sub>: Oxalic acid modified TiO<sub>2</sub>; c) EDA-TiO<sub>2</sub>: Ethylenediamine modified TiO<sub>2</sub>; d) DLA-TiO<sub>2</sub>: DL-Alanine modified TiO<sub>2</sub>.

The TG results were also analyzed to prove the organic groups existence in the functional TiO<sub>2</sub> samples (Fig. 2). For the P25, there is no weight lost at all TG test temperature except for very little loss of adsorbed water. For all the functional TiO<sub>2</sub>

samples, the first thermal degradation step losing of around 15.0 wt% below 200°C is attributed to the loss of adsorbed water. The second thermal degradation step after 200°C is possibly ascribed to the decomposition of the organic groups on the TiO<sub>2</sub> samples [15]. For the OAD-TiO<sub>2</sub> and DLA-TiO<sub>2</sub>, the second step is a simple and similar weight loss about 5.0%, however, the EDA-TiO<sub>2</sub> exhibits different weight loss (9.0 wt%) at the same range of temperature (200-540°C). The above results are attributed to the thermal decomposition of the organics from the hydrolysis of titanium (IV) butoxide precursor, carboxylic and hydroxyl groups on the functional TiO<sub>2</sub> surface. The weight loss results reveal the different organic contents in different samples. The weight loss step over 540°C is considered as the loss of amino groups on the surface of EDA-TiO<sub>2</sub>. The TG result indicates that there are several functional groups on the modified TiO<sub>2</sub> surface and the interaction between organic groups and TiO<sub>2</sub> in EDA-TiO<sub>2</sub> is different from that of OAD-TiO<sub>2</sub> and DLA-TiO<sub>2</sub>, which is similar with the result of FT-IR test.

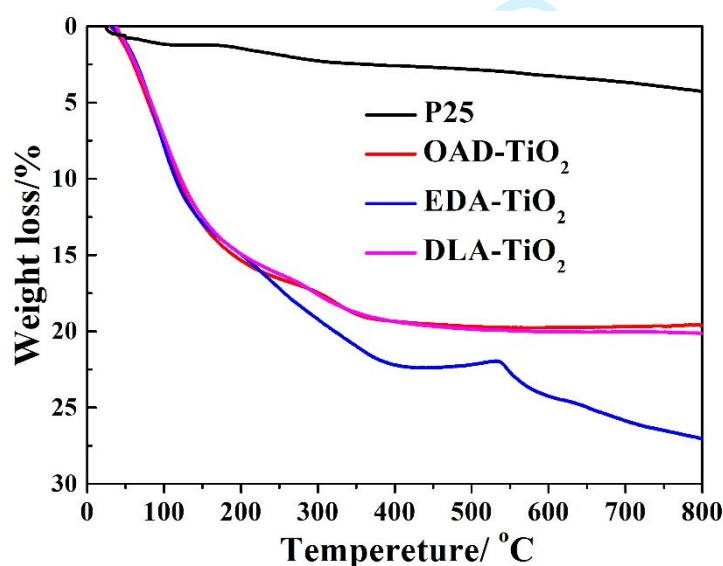


Figure 2. TG spectra of the TiO<sub>2</sub> samples.

The zeta potential of the modified  $\text{TiO}_2$  samples under different solution pH is shown in Fig. 3. The isoelectric point ( $\text{pH}_{\text{iep}}$ ) is the pH value of the solution when the zeta potential is zero. The  $\text{pH}_{\text{iep}}$  values of the functional  $\text{TiO}_2$  samples decreased intensely after modified by carboxyl and amino groups. The OAD- $\text{TiO}_2$  sample exhibited lower  $\text{pH}_{\text{iep}}$  value than others. This can be deduced that the carboxyl group in OAD make its surface negatively charged easily. The  $\text{TiO}_2$  samples are gradually more positively charged while the increasing number of amino groups were introduced into the functional  $\text{TiO}_2$  samples like DLA- $\text{TiO}_2$  and EDA- $\text{TiO}_2$ . In addition, the  $\text{pH}_{\text{iep}}$  of functionalized samples are all less than that of P25. The value of zeta potential of adsorbents materials should be focused on because this parameter could affect the interaction between  $\text{TiO}_2$  samples and contaminants[27]. In fact, lower  $\text{pH}_{\text{iep}}$  for sample is not favorable to enhance the adsorption efficiency of anions such as ARG. Therefore, the adsorption capacity of modified  $\text{TiO}_2$  will be compared with that of P25 in the “adsorption mechanism” to find the role of electrostatic attraction in the adsorption process.

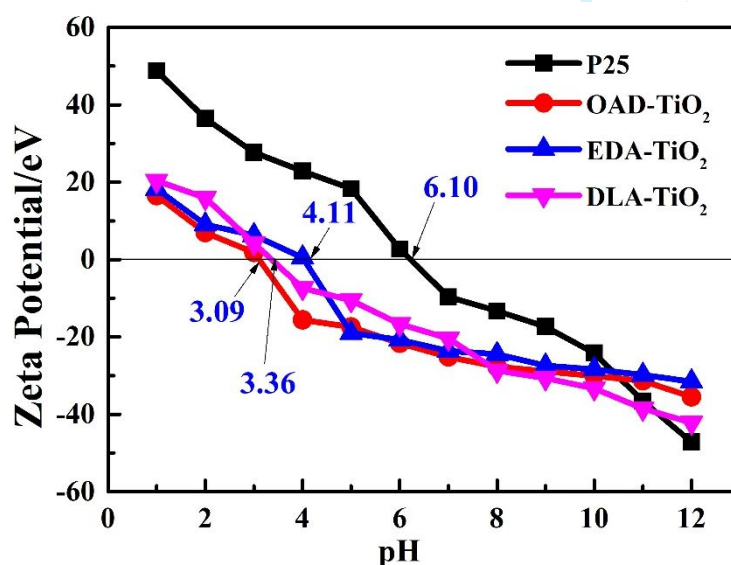


Figure 3. Zeta potential of the TiO<sub>2</sub> samples. (The numbers in blue mean isoelectronic point)

The BET surface area ( $S_{BET}$ ), pore volume ( $V_p$ ) and pore diameter parameters of the TiO<sub>2</sub> samples are listed in Table 2. The  $S_{BET}$  and pore diameter were calculated from the corresponding nitrogen adsorption-desorption isotherms and the desorption branch of the nitrogen isotherms by the BJH (Fig. S2). It can be seen from the data that the  $S_{BET}$  of the OAD-TiO<sub>2</sub> and EDA-TiO<sub>2</sub> are smaller than that of the P25, while the  $S_{BET}$  of the DLA-TiO<sub>2</sub> is larger than the value of P25. The phenomenon can be explained by the fact that the  $S_{BET}$  of the TiO<sub>2</sub> samples greatly depends on the size of the aggregated TiO<sub>2</sub> particles, which is consistent with the result of SEM (Fig. S1). The  $V_p$  value also exhibits the similar variation tendency. The agglomeration of the organic components might cause the collapse of the porous structure and then led to the decrease of pore volume [28]. Furthermore, the hysteresis between the adsorption and desorption curves for OAD-TiO<sub>2</sub> illustrates the diffusion bottleneck in its tissue, probably owing to heterogeneous pore size. The pore radius of the samples calculated by the BJH method was in a narrow range of 1.0-9.0 nm, which indicates that all the TiO<sub>2</sub> samples have mesoporous and microporous structures. Such structures are attributed to the pores which are formed between TiO<sub>2</sub> particles[29]. From the result, it can be seen that the specific surface area of DLA-TiO<sub>2</sub> is much larger than that of OAD-TiO<sub>2</sub> and EDA-TiO<sub>2</sub>, which is probably relative to the microporous structure [30]. These results indicate that the functional groups dramatically influence the surface texture of the functional TiO<sub>2</sub> samples.

Table 2. Textural properties of the TiO<sub>2</sub> samples.

Sample	$S_{BET}/m^2 \cdot g^{-1}$	$V_p/cm^3 \cdot g^{-1}$	$R/nm$
P25 <sup>a)</sup>	48.48	0.258	1.07
OAD-TiO <sub>2</sub> <sup>b)</sup>	30.47	0.043	2.88
EDA-TiO <sub>2</sub> <sup>c)</sup>	25.56	0.188	8.92
DLA-TiO <sub>2</sub> <sup>d)</sup>	401.26	0.366	1.83

a) P25: commercial bare TiO<sub>2</sub>; b) OAD-TiO<sub>2</sub>: Oxalic acid modified TiO<sub>2</sub>; c) EDA-TiO<sub>2</sub>: Ethylenediamine modified TiO<sub>2</sub>; d) DLA-TiO<sub>2</sub>: DL-Alanine modified TiO<sub>2</sub>.

### 3.2. Effect of pH

The initial solution pH is one of the most important factors for the adsorption process. The interaction between adsorbent and adsorbate could be effectively affected by the solution pH variation due to the change of surface characteristics for the adsorbent or the change of the form of adsorbates [31]. In this study, the ARG adsorption capacity onto the TiO<sub>2</sub> samples is dramatically influenced by the initial solution pH value (Fig. 4). The adsorption capacity is higher at low pH value and exhibits a sharp decline when the pH value is over the  $pH_{iep}$ . The positively charged surface of the samples and anionic nature of ARG indicate that the electrostatic interaction between ARG and the TiO<sub>2</sub> samples might play a meaningful role in adsorption process. However, it is obvious that P25 exhibits much lower adsorption capacity than other functional samples even it possesses a higher  $pH_{iep}$  value. This result suggests that electrostatic attraction is an important factor for the adsorption capacity of the modified samples but not the decisive reason for the enhanced adsorption performance.



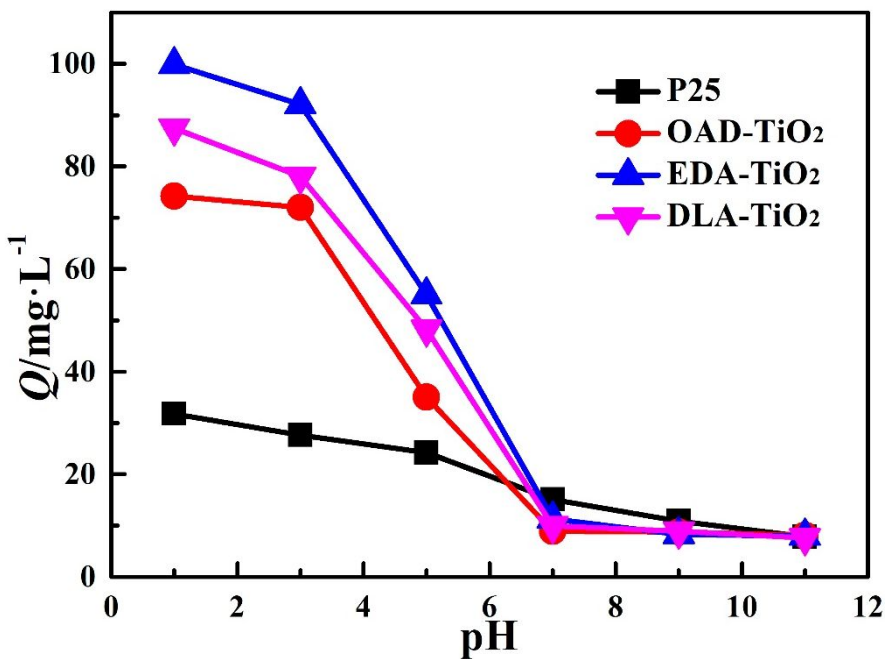


Figure 4. Influence of the solution pH on the ARG adsorption onto the TiO<sub>2</sub> samples.

Experimental conditions: initial ARG C<sub>0</sub> 200 mg/L, dosage 2 g/L.

3.3. Adsorption kinetics

The adsorption kinetics of ARG onto the TiO<sub>2</sub> samples were studied by employing the initial ARG concentrations in the range of 100, 200 and 300 mg/L. The correlation between adsorption time and adsorption capacity of ARG at different initial concentrations are shown in the Fig. 5. As expected, the adsorption capacity increases as the time goes on and finally reaches a plateau, which indicates that the dynamic equilibrium between the adsorption and desorption was reached and no more molecules would be adsorbed even though the contact time prolonged. A very interesting result can be announced that the functional TiO<sub>2</sub> samples have a shorter equilibrium time than that of P25. The adsorption equilibrium of the functional TiO<sub>2</sub> samples can be reached within 20 min in all the used concentrations while the value for P25 is more than 40 min. This phenomenon indicates that the functional carboxyl and amino groups on the



surface of the  $\text{TiO}_2$  samples possesses a very obvious effect on the adsorption kinetics of ARG, which is consistent with the result of 'the reports'. [32-34]. The adsorption kinetics of ARG onto P25 and the functional  $\text{TiO}_2$  samples are also displayed in Fig. 5 and the corresponding parameters fitted by the pseudo-first-order and pseudo-second-order model are listed in Table 3. The adsorption behavior of ARG onto the four  $\text{TiO}_2$  samples can be well described by the pseudo-second-order model ( $R^2=0.9919-0.9997$ ). Furthermore, the calculated values of  $Q_e$  from the pseudo-second-order model are approximately equal to the experimental values ( $Q_{exp}$ ). This indicates that the adsorption kinetics of ARG onto the  $\text{TiO}_2$  samples corresponds well with the pseudo-second-order model and the adsorption process is mainly dominated by chemical reaction [35].

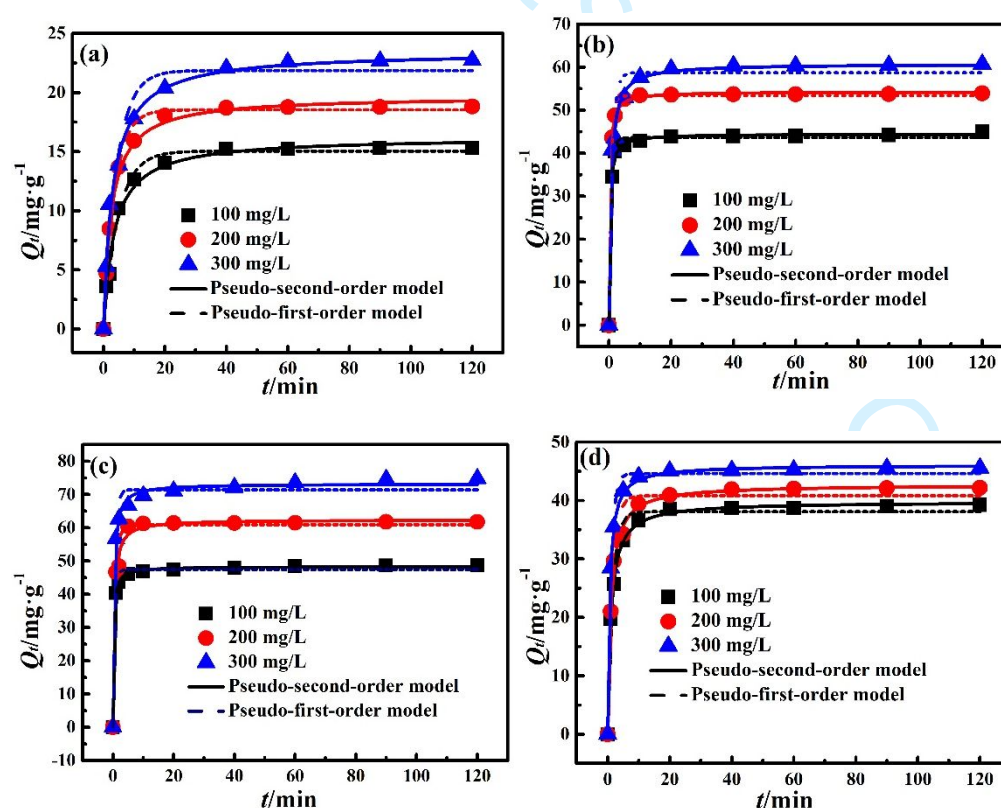


Figure 5. Kinetics plots of ARG adsorbed onto (a) P25, (b) DLA- $\text{TiO}_2$ , (c) EDA- $\text{TiO}_2$

1  
2  
3  
4 310 and (d) OAD-TiO<sub>2</sub>. Experimental conditions: initial C<sub>0</sub> 100, 200, 300 mg/L, solution  
5  
6 311 pH 3.0, dosage 2 g/L.  
7

8 312 Table 3. Kinetics parameters for ARG adsorption at different initial concentrations.

9

Sample	C <sub>0</sub> /mg·L <sup>-1</sup>	Q <sub>exp</sub> /mg·g <sup>-1</sup>	pseudo-first-order model			pseudo-second-order model		
			k <sub>1</sub> /l·min <sup>-1</sup>	Q <sub>e</sub> /mg·g <sup>-1</sup>	R <sup>2</sup>	k <sub>2</sub> /g·(min·mg) <sup>-1</sup>	Q <sub>e</sub> /mg·g <sup>-1</sup>	R <sup>2</sup>
P25 <sup>a)</sup>	100	15.83	0.208	15.04	0.9894	0.018	16.22	0.9919
	200	18.82	0.273	18.53	0.9926	0.020	19.09	0.9947
	300	22.72	0.229	21.86	0.9714	0.014	23.15	0.9953
OAD-TiO <sub>2</sub> <sup>b)</sup>	100	39.24	0.605	38.07	0.9832	0.024	39.78	0.9989
	200	42.17	0.640	40.81	0.9766	0.023	42.70	0.9975
	300	45.55	0.905	44.62	0.9904	0.036	46.08	0.9992
EDA-TiO <sub>2</sub> <sup>c)</sup>	100	48.71	1.791	47.46	0.9923	0.101	48.28	0.9986
	200	61.78	1.195	60.93	0.9773	0.042	62.40	0.9996
	300	74.77	1.430	71.42	0.9810	0.043	73.21	0.9997
DLA-TiO <sub>2</sub> <sup>d)</sup>	100	44.98	1.511	43.59	0.9952	0.084	44.45	0.9983
	200	53.93	1.610	53.33	0.9963	0.079	54.24	0.9994
	300	60.69	0.923	58.71	0.9637	0.027	60.77	0.9929

13  
14  
15  
16  
17  
18  
19  
20  
21  
22  
23  
24  
25  
26  
27  
28  
29

30 313 a) P25: commercial bare TiO<sub>2</sub>; b) OAD-TiO<sub>2</sub>: Oxalic acid modified TiO<sub>2</sub>; c) EDA-TiO<sub>2</sub>:  
31 314 Ethylenediamine modified TiO<sub>2</sub>; d) DLA-TiO<sub>2</sub>: DL-Alanine modified TiO<sub>2</sub>.  
32  
33

34 315 **3.4. Adsorption isotherms**

35  
36 316 The adsorption isotherm study plays an important role in understanding the  
37  
38 317 adsorption mechanism. The surface stacking of the adsorbates onto the adsorbent could  
39  
40 318 be considered as a monolayer or multilayer state due to the isotherm models [36].  
41  
42 319 Herein, two common adsorption isotherm models, Freundlich and Langmuir models,  
43  
44 320 were used to fit the experimental data at 25°C. The corresponding experimental data  
45  
46 321 and fitting curves of Langmuir and Freundlich models are shown in Fig. 6 (the isotherm  
47  
48 322 fitting models at different temperature are shown in Fig. S3), the fitting parameters are  
49  
50 323 listed in Table 4 (the isotherm fitting parameters at different temperature are list in  
51  
52 324 Table S1). It is obvious that Langmuir model is more reasonable to describe the  
53  
54  
55  
56  
57  
58  
59  
60

adsorption process of ARG onto P25 and the functional TiO<sub>2</sub> samples than Freundlich model according to the value of correlation coefficient ( $R^2$ ), which significantly indicates that the adsorption sites on the surface of the TiO<sub>2</sub> samples are uniform and the adsorption of ARG onto the surface of the TiO<sub>2</sub> samples is monolayer [37]. The adsorption capacity of the functionalized TiO<sub>2</sub> samples for ARG obtained from the Langmuir model is larger than that of P25. Meanwhile, the adsorption capacity of DLA-TiO<sub>2</sub> is not higher than that of EDA-TiO<sub>2</sub>, although DLA-TiO<sub>2</sub> has the larger specific surface area. The above result could be explained as follows: the partial specific surface area of DLA-TiO<sub>2</sub> comes from the microporous structure, while the ARG molecule is too large to enter the nanoscale pore structure for adsorption [38]. Moreover, the values of  $R_L$  are from 0.0143-0.1538 (in the range of 0-1.0), the values of  $1/n$  are 0.122-0.323, which suggests that the adsorption of ARG onto the functional TiO<sub>2</sub> surface is favorable. Furthermore, the values of  $R_L$  and  $1/n$  for the functional TiO<sub>2</sub> samples are smaller than that of P25, indicating that the modified TiO<sub>2</sub> samples are prone to be the adsorption of ARG.

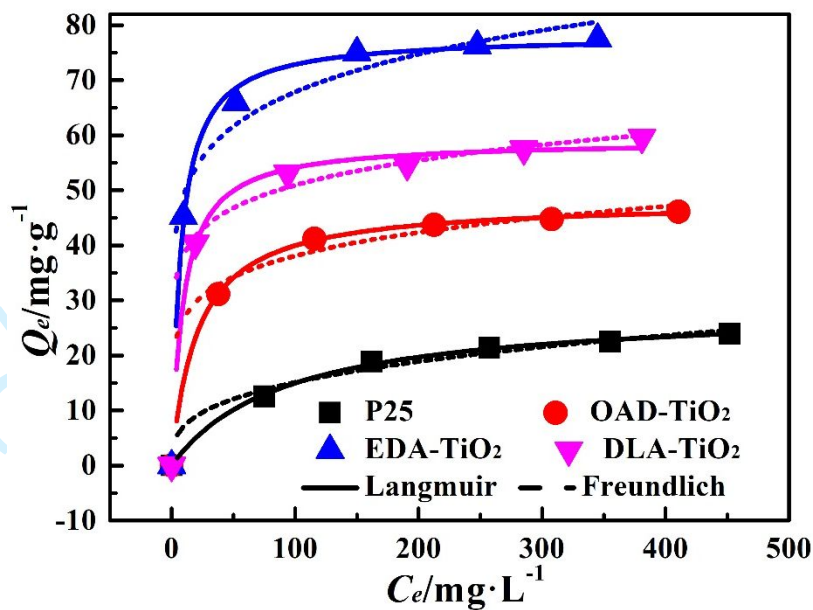


Figure 6. Adsorption isotherms for ARG adsorbed onto the TiO<sub>2</sub> samples at 25°C. Experimental conditions: initial ARG C<sub>0</sub>=10-500 mg/L, solution pH 3.0, contact time 120 min.

Table 4. Langmuir, and Freundlich isotherm parameters for ARG adsorbed onto the TiO<sub>2</sub> samples.

Samples	$R_L$	Langmuir model parameters			Freundlich model parameters		
		$Q_{m,cal}/\text{mg}\cdot\text{g}^{-1}$	$K_L/\text{L}\cdot\text{mg}^{-1}$	$R^2$	$K_F(\text{mg/g})\cdot(\text{mg/L})^{-n}$	$1/n$	$R^2$
P25 <sup>a)</sup>	0.1538	28.78	0.011	0.9903	3.42	0.323	0.9293
OAD-TiO <sub>2</sub> <sup>b)</sup>	0.0392	48.11	0.049	0.9969	18.86	0.153	0.9036
EDA-TiO <sub>2</sub> <sup>c)</sup>	0.0143	78.15	0.138	0.9840	35.79	0.139	0.9078
DLA-TiO <sub>2</sub> <sup>d)</sup>	0.0180	59.07	0.109	0.9567	29.01	0.122	0.9484

a) P25: commercial bare TiO<sub>2</sub>; b) OAD-TiO<sub>2</sub>: Oxalic acid modified TiO<sub>2</sub>; c) EDA-TiO<sub>2</sub>: Ethylenediamine modified TiO<sub>2</sub>; d) DLA-TiO<sub>2</sub>: DL-Alanine modified TiO<sub>2</sub>.

3.5. Regeneration performance of TiO<sub>2</sub> samples

To study the regeneration performance of the functional TiO<sub>2</sub> samples, NaOH solution(0.1 mol/L) and HNO<sub>3</sub> solution(0.1 mol/L) were employed as the desorption agent and the regeneration agent respectively because the adsorption capacity of ARG onto the TiO<sub>2</sub> samples is strongly pH dependent. The regenerated adsorbent (2 g/L) was

reused to adsorb ARG (200 mg/L) at 25°C, and the results of the adsorption capacity change versus the recycles are presented in Fig. 7. It is obvious that there is little loss of the adsorption capacity of the functional TiO<sub>2</sub> samples for ARG after five adsorption-desorption cycles. It is illustrated that the interactions between the functional TiO<sub>2</sub> samples and ARG can be destroyed by dilute NaOH solution and the adsorption ability of the functional TiO<sub>2</sub> samples can be easily regenerated. The above results of the regeneration suggest functional TiO<sub>2</sub> is a promising adsorbent in the removal of ARG dye.

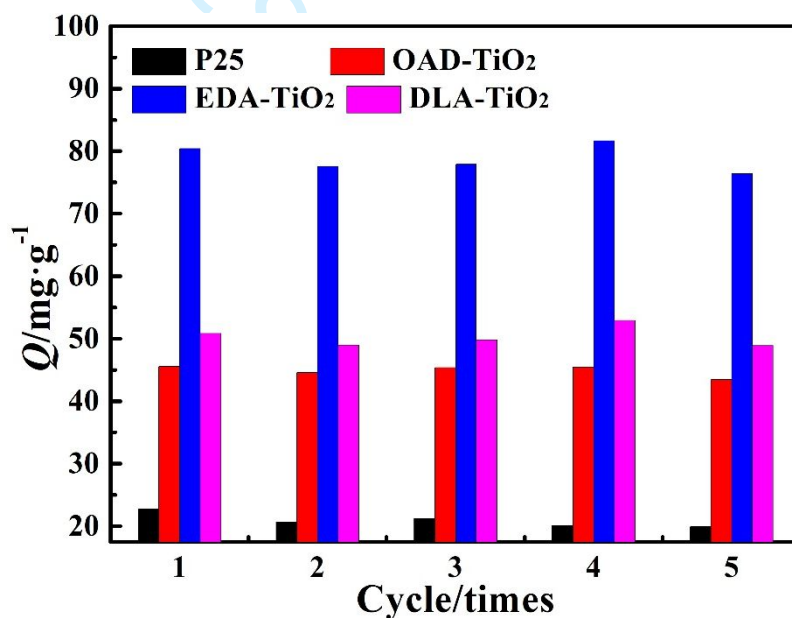


Figure 7. Recycle performance of the TiO<sub>2</sub> samples with the initial concentrations of 200 mg/L of ARG, contact time of 120 min, at the temperature of 25°C.

### 3.6. Adsorption mechanism

The result of the isotherm and kinetics experiments reveals the adsorption capacity of three functionalized TiO<sub>2</sub> samples were at the order of EDA (with two amino groups)-TiO<sub>2</sub> > DLA (with one amino group and one carboxyl group)-TiO<sub>2</sub> > OAD (with

two carboxyl groups)-TiO<sub>2</sub>, which is consistent with the result of the pH<sub>iep</sub> test. OAD with two carboxyl groups in the molecule structure makes the TiO<sub>2</sub> negatively charged easily. With the amino group introduced, the pH<sub>iep</sub> of samples is much larger than that of OAD-TiO<sub>2</sub> because the amino group is easy to protonate so that it carries more positive charges on the surface of TiO<sub>2</sub>. Meanwhile, ARG is a typical anionic dye, which is easily adsorbed by the adsorbent with more positive charge. Therefore, the adsorption capacity of the functional TiO<sub>2</sub> samples is in accordance with the above order. However, it is also obvious that the adsorption capacity of P25 is less than all of the functional samples though the pH<sub>(iep)</sub> of P25 is largest in the samples. This result illustrate that though electrostatic attraction makes contribution to the impact for the adsorption capacity, there are also some more important factors for the adsorption mechanisms. Therefore, the FTIR analysis were used to find more precise conclusion.

The FT-IR spectra of the three TiO<sub>2</sub> samples before and after the adsorption of ARG are presented in Fig. 8. It is illustrated that the obvious shifting of peaks occurred, and some new peaks related to ARG appeared after adsorption process. In detail, the peaks of 1496 cm<sup>-1</sup>( $\nu_{C=C}$  for benzenoid rings in ARG molecule), 1218 cm<sup>-1</sup> ( $\nu_{=N-C}$  connect with phenyl), and 1045 cm<sup>-1</sup>( $\nu_{S=O}$  for the -SO<sub>3</sub><sup>-</sup> in ARG molecule) [39, 40] appeared after adsorbed by all the three functional TiO<sub>2</sub> samples, respectively. These peaks illustrate that ARG was successfully adsorbed onto the functional TiO<sub>2</sub> samples. Meanwhile, the peak 1690 cm<sup>-1</sup> ( $\nu_{C=O}$ ) in OAD-TiO<sub>2</sub> and the peak 1510 cm<sup>-1</sup>( $\nu_{N-H}$  in the secondary amino) in DLA-TiO<sub>2</sub> and EDA-TiO<sub>2</sub> disappeared, which indicates that there are interactions between ARG and the carboxyl or amino groups in the TiO<sub>2</sub>

samples during the adsorption. In addition, the adsorption performance of EDA-TiO<sub>2</sub> is better than DLA-TiO<sub>2</sub> and OAD-TiO<sub>2</sub> according to the experimental data. The above results demonstrate that functional groups, especially amino groups play an important role in the adsorption of ARG, which could also account for the poor adsorption capacity of P25.

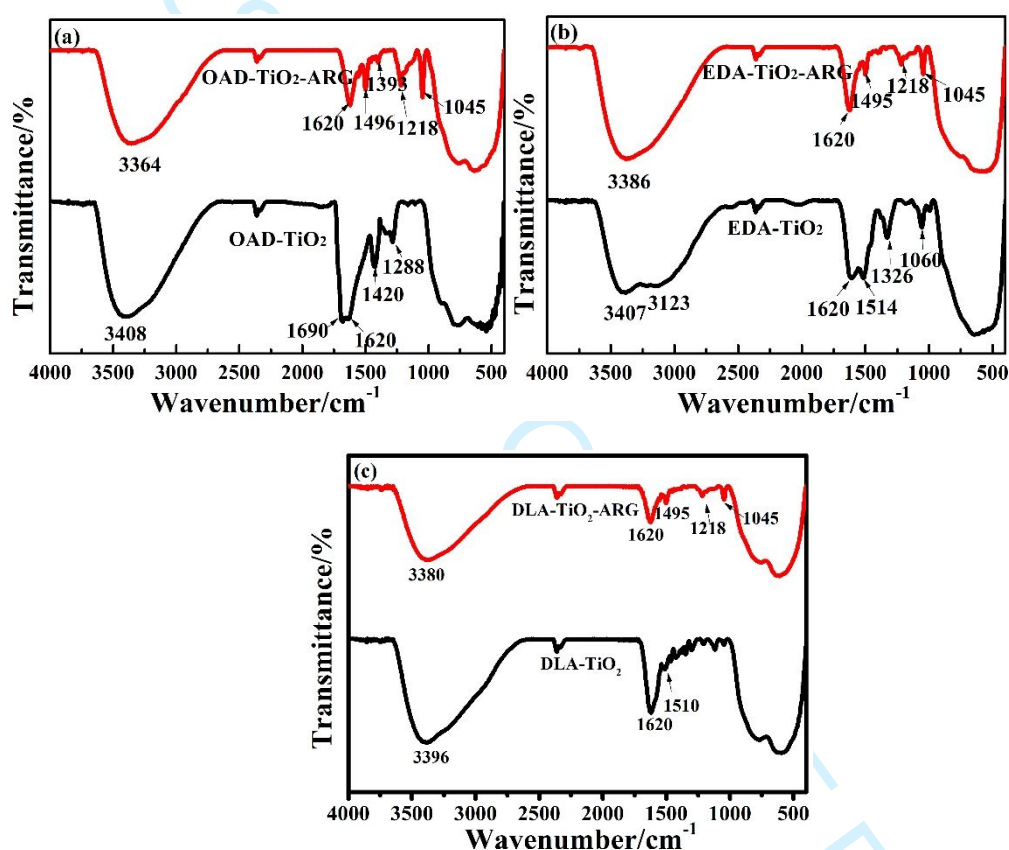


Figure 8. FTIR spectra of (a) OAD-TiO<sub>2</sub>, (b) EDA-TiO<sub>2</sub>, and (c) DLA-TiO<sub>2</sub> before and after adsorption of ARG. (the data before and after adsorption of ARG are represented by black and red curves, respectively)

According to the previous analysis and literatures [41, 42], the interaction between ARG and functional groups especially amino group made the main contribution to the adsorption of organic dye onto the modified TiO<sub>2</sub> samples, and electrostatic interaction is also involved in this process. In the desorption process, these interactions could be



destroyed easily in the alkaline solution, which results in the desorption of ARG from the modified TiO<sub>2</sub> samples.

#### 4. Conclusions

The interfacial functionalized TiO<sub>2</sub> samples with carboxyl and amino groups were successfully prepared at lower temperature by using hydrolysis method and exhibited an enhanced adsorption performance for removal of anionic dye ARG from aqueous solution. The carboxyl group combined into the TiO<sub>2</sub> with bridging and chelating structure, while the amino group anchored into the TiO<sub>2</sub> with hydrogen bonding. The introduction of carboxyl and amino groups had a significant effect on the physicochemical properties of the functional TiO<sub>2</sub>, such as surface charge, thermal stability, surface texture, and further influenced the adsorption performance of the functionalized TiO<sub>2</sub> samples for anionic dye ARG. The functionalized TiO<sub>2</sub> displays a higher adsorption capacity, faster adsorption rate and better regeneration than that of P25. The EDA modified TiO<sub>2</sub> has the maximum adsorption capacity for ARG as 78.15 mg/g, while that of DLA-TiO<sub>2</sub> is 59.07 mg/g, and the OAD-TiO<sub>2</sub> is 48.11 mg/g. We find that the main adsorption mechanism is the interaction between ARG and amino groups or carboxyl groups and the surface charge is also related to this process. In summary, the carboxyl and amino groups in the functional TiO<sub>2</sub> have dramatic influence on the physicochemical properties of TiO<sub>2</sub>, and further impact the adsorption performance. This discovery could provide a powerful proof for the design of some specific adsorbent for organic dyes removal.

#### Acknowledgments



The authors gratefully acknowledge the Shaanxi Key research and development projects, China (Grant No. 2017SF-386), the Fundamental Research Funds for the Central Universities of China and the Key Industrial Project in Xianyang City, Shaanxi, China (Grant No.2018k02-10).

#### Appendix A. Supplementary data

Table S1. Langmuir, and Freundlich isotherm parameters for ARG adsorbed onto the TiO<sub>2</sub> samples at different temperature.

Fig. S1. SEM images and EDX spectra of the TiO<sub>2</sub> samples.

Fig. S2. Nitrogen adsorption-desorption isotherms (Inset are the pore size distribution) of the TiO<sub>2</sub> samples.

Fig. S3. Adsorption isotherms for ARG adsorbed onto the TiO<sub>2</sub> samples at different temperature fitting with Langmuir and Freundlich models.

#### References

1. Park H, Kim H I, Moon G H, Choi W. Photoinduced charge transfer processes in solar photocatalysis based on modified TiO<sub>2</sub>. *Energy & Environmental Science*, 2016, 9(2): 411-433
2. Nakata K, Fujishima A. TiO<sub>2</sub> photocatalysis: Design and applications. *Journal of Photochemistry and Photobiology C: Photochemistry Reviews*, 2012, 13(3): 169-189
3. Schneider J, Matsuoka M, Takeuchi M, Zhang J, Horiuchi Y, Anpo M, Bahnemann D W. Understanding TiO<sub>2</sub> photocatalysis: mechanisms and materials. *Chemical Reviews*, 2014, 114(19): 9919-9986
4. Xu H, Ouyang S, Liu L, Reunchan P, Umezawa N, Ye J. Recent advances in TiO<sub>2</sub>-based photocatalysis. *Journal of Materials Chemistry A*, 2014, 2(32): 12642-12661
5. Prieto Rodriguez L, Miralles Cuevas S, Oller I, Aguera A, Li Puma G, Malato S. Treatment of emerging contaminants in wastewater treatment plants (WWTP) effluents by solar photocatalysis using low TiO<sub>2</sub> concentrations. *Journal of Hazardous*

- Materials, 2012, 211: 131-137
6. Marinho B A, Cristóvão R O, Djellabi R, Loureiro J M, Boaventura R A, Vilar V J P. Photocatalytic reduction of Cr(VI) over TiO<sub>2</sub>-coated cellulose acetate monolithic structures using solar light. *Applied Catalysis B: Environmental*, 2017, 203: 18-30
7. Choi Y, Koo M S, Bokare A D, Kim D H, Bahnemann D W, Choi W. Sequential process combination of photocatalytic oxidation and dark reduction for the removal of organic pollutants and Cr(VI) using Ag/TiO<sub>2</sub>. *Environmental Science & Technology*, 2017, 51(7): 3973-3981
8. Xiong L, Sun W, Yang Y, Chen C, Ni J. Heterogeneous photocatalysis of methylene blue over titanate nanotubes: effect of adsorption. *Journal of Colloid and Interface Science*, 2011, 356(1): 211-216
9. Nguyen Phan T D, Song M B, Shin E W. Removal efficiency of gaseous benzene using lanthanide-doped mesoporous titania. *Journal of Hazardous Materials*, 2009, 167(1-3): 75-81
10. Zhang L, Cole J M, Dai C. Variation in optoelectronic properties of azo dye-sensitized TiO<sub>2</sub> semiconductor interfaces with different adsorption anchors: carboxylate, sulfonate, hydroxyl and pyridyl groups. *ACS Applied Materials & Interfaces*, 2014, 6(10): 7535-7546
11. Kim B, Park S W, Kim J Y, Yoo K, Lee J A, Lee M W, Lee D K, Kim J Y, Kim B, Kim H, et al. Rapid dye adsorption via surface modification of TiO<sub>2</sub> photoanodes for dye-sensitized solar cells. *ACS Applied Materials & Interfaces*, 2013, 5(11): 5201-5207
12. Natarajan T S, Bajaj H C, Tayade R J. Preferential adsorption behavior of methylene blue dye onto surface hydroxyl group enriched TiO<sub>2</sub> nanotube and its photocatalytic regeneration. *Journal of Colloid and Interface Science*, 2014, 433: 104-114
13. Sugita T, Kobayashi K I, Kobayashi K, Yamazaki T, Fujii K, Itabashi H, Mori M. Enhanced aqueous adsorption and photodecomposition of anionic organic target by amino group-modified TiO<sub>2</sub> as anionic adsorptive photocatalyst. *Journal of*

- Photochemistry and Photobiology A: Chemistry, 2018, 356: 71-80
14. Baig M I, Ingole P G, Choi W K, Park S R, Kang E C, Lee H K. Development of carboxylated TiO<sub>2</sub> incorporated thin film nanocomposite hollow fiber membranes for flue gas dehydration. *Journal of Membrane Science*, 2016, 514: 622-635
15. Minh Tri N L, Byeong Kyu L. High temperature synthesis of interfacial functionalized carboxylate mesoporous TiO<sub>2</sub> for effective adsorption of cationic dyes. *Chemical Engineering Journal*, 2015, 281: 20-33
16. Liu J M, Han L, An N, Xing L, Ma H Y, Cheng L, Yang J C, Zhang Q C. Enhanced visible-light photocatalytic activity of carbonate-doped anatase TiO<sub>2</sub> based on the electron-withdrawing bidentate carboxylate linkage. *Applied Catalysis B: Environmental*, 2017, 202: 642-652
17. Wang J, Yang G, Chen J, Liu Y, Wang Y, Lao C Y, Xi K, Yang D, Harris C J, Yan W, et al. Flexible and High-loading lithium-sulfur batteries enabled by integrated three-in-one fibrous membranes. *Advanced Energy Materials*, 2019, 9(38): doi.org/10.1002/aenm.201902001
18. Weng Y, Li L, Liu Y, Wang L, Yang G. Surface-binding forms of carboxylic groups on nanoparticulate TiO<sub>2</sub> surface studied by the interface-sensitive transient triplet-state molecular probe. *Journal of Physical Chemistry B*, 2003, 107(18): 4356-4363
19. Karapati S, Giannakopoulou T, Todorova N, Boukos N, Dimotikali D, Trapalis C. Eco-efficient TiO<sub>2</sub> modification for air pollutants oxidation. *Applied Catalysis B: Environmental*, 2015, 176-177: 578-585
20. Mallakpour S, Nikkhoo E. Surface modification of nano-TiO<sub>2</sub> with trimellitylimido-amino acid-based diacids for preventing aggregation of nanoparticles. *Advanced Powder Technology*, 2014, 25(1): 348-353
21. Shi B, Zhao C, Ji Y, Shi J, Yang H. Promotion effect of PANI on Fe-PANI/Zeolite as an active and recyclable Fenton-like catalyst under near-neutral condition. *Applied Surface Science*, 2020, 508: doi.org/10.1016/j.apsusc.2020.145298
22. Li X, Wang D, Cheng G, Luo Q, An J, Wang Y. Preparation of polyaniline-

- modified TiO<sub>2</sub> nanoparticles and their photocatalytic activity under visible light illumination. *Applied Catalysis B: Environmental*, 2008, 81: 267-273
23. Janković I A, Šaponjić Z V, Čomor M I, Nedeljković J M. Surface modification of colloidal TiO<sub>2</sub> nanoparticles with bidentate benzene derivatives. *Journal of Physical Chemistry C*, 2009, 113: 12645–12652
24. WDuckworth O, TMartin S. Surface complexation and dissolution of hematite by C1-C6 dicarboxylic acids at pH=5.0. *Geochimica et Cosmochimica Acta*, 2001, 65(23): 4289-4301
25. D.Filius J, Hiemstra T, H. Van Riemsdijk W. Adsorption of small weak organic acids on goethite: Modeling of mechanisms. *Journal of Colloid and Interface Science*, 1997, 195(2): 368-380
26. Crake A, Christoforidis K C, Godin R, Moss B, Kafizas A, Zafeiratos S, Durrant J R, Petit C. Titanium dioxide/carbon nitride nanosheet nanocomposites for gas phase CO<sub>2</sub> photoreduction under UV-visible irradiation. *Applied Catalysis B: Environmental*, 2019, 242: 369-378
27. Feng J, Zhu J, Lv W, Li J, Yan W. Effect of hydroxyl group of carboxylic acids on the adsorption of Acid Red G and Methylene Blue on TiO<sub>2</sub>. *Chemical Engineering Journal*, 2015, 269: 316-322
28. Yu J C, Yu J G, Ho W K, Jiang Z T, Zhang L Z. Effects of F<sup>-</sup> doping on the photocatalytic activity and microstructures of nanocrystalline TiO<sub>2</sub> powders. *Chemistry of Materials*, 2002, 14(9): 3808-3816
29. Yu J C, Yu J G, Ho W K, Zhang L Z. Preparation of highly photocatalytic active nano-sized TiO<sub>2</sub> particles via ultrasonic irradiation. *Chemical Communications*, 2001, 19: 1942-1943
30. Lyu W, Wu J M, Zhang W L, Liu Y P, Yu M T, Zhao Y F, Feng J T, Yan W. Easy separated 3D hierarchical coral-like magnetic polyaniline adsorbent with enhanced performance in adsorption and reduction of Cr(VI) and immobilization of Cr(III). *Chemical Engineering Journal*, 2019, 363: 107-119
31. Moreno Castilla C. Adsorption of organic molecules from aqueous solutions

- on carbon materials. *Carbon*, 2004, 42(1): 83-94
32. Shayegan Z, Haghighat F, Lee C S, Bahloul A, Huard M. Effect of surface fluorination of P25-TiO<sub>2</sub> on adsorption of indoor environment volatile organic compounds. *Chemical Engineering Journal*, 2018, 346: 578-589
33. Li S, Fang L, Ye M, Zhang Y. Enhanced adsorption of norfloxacin on modified TiO<sub>2</sub> particles prepared via surface molecular imprinting technique. *Desalination and Water Treatment*, 2016, 57: 408-418
34. Leong S, Li D, Hapgood K, Zhang X W, Wang H T. Ni(OH)<sub>2</sub> decorated rutile TiO<sub>2</sub> for efficient removal of tetracycline from wastewater. *Applied Catalysis B: Environmental*, 2016, 198: 224-233
35. Wang L, Wang J, Wang Z, He C, Lyu W, Yan W, Yang L. Enhanced antimonate (Sb(V)) removal from aqueous solution by La-doped magnetic biochars. *Chemical Engineering Journal*, 2018, 354: 623-632
36. Srinivasan A, Viraraghavan T. Decolorization of dye wastewaters by biosorbents: a review. *Journal of Environment Management*, 2010, 91(10): 1915-1929
37. Zhang W L, Fu R, Wang L, Zhu J W, Feng J T, Yan W. Rapid removal of ammonia nitrogen in low-concentration from wastewater by amorphous sodium titanate nano-particles. *Science of the Total Environment*, 2019, 668: 815-824
38. Suresh Kumar P, Korving L, Keesman K J, van Loosdrecht M, Witkamp G. Effect of pore size distribution and particle size of porous metal oxides on phosphate adsorption capacity and kinetics. *Chemical Engineering Journal*, 2019, 358: 160-169
39. Han X X, Zhu G Q, Ding Y X, Miao Y L, Wang K W, Zhang H J, Wang Y b, Liu S B. Selective catalytic synthesis of glycerol monolaurate over silica gel-based sulfonic acid functionalized ionic liquid catalysts. *Chemical Engineering Journal*, 2019, 359: 733-745
40. Han X, Yan W, Hung C T, He Y, Wu P H, Liu L L, Huang S J, Liu S B. Transesterification of soybean oil to biodiesel by tin-based Brønsted-Lewis acidic ionic liquid catalysts. *Korean Journal of Chemical Engineering*, 2016, 33(7): 2063-2072
41. Zhang X, Bai R. Adsorption behavior of humic acid onto polypyrrole-coated

571 nylon 6,6 granules. Journal of Materials Chemistry, 2002, 12(9): 2733-2739

572 42. Li J, Zhang Q, Feng J, Yan W. Synthesis of PPy-modified TiO<sub>2</sub> composite in

573 H<sub>2</sub>SO<sub>4</sub> solution and its novel adsorption characteristics for organic dyes. Chemical

574 Engineering Journal, 2013, 225: 766-775

575

## Insight into the Effect of Surface Carboxyl and Amino Groups on the Adsorption of Titanium Dioxide for Acid Red G

Wenlong Zhang<sup>1</sup>, Xuyang Zhao<sup>1</sup>, Lin Zhang<sup>1</sup>, Jinwei Zhu<sup>1,2</sup>, Shanshan Li<sup>1</sup>, Ping Hu<sup>3</sup>, Jiangtao Feng<sup>1\*</sup>, Wei Yan<sup>1</sup>

<sup>1</sup>Department of Environmental Science and Engineering, Xi'an Jiaotong University, Xi'an 710049, P.R. China

<sup>2</sup>Shaanxi Electrical Equipment Institution, Xi'an 710025, P.R. China

<sup>3</sup>Shaanxi Polytechnic Institute, Xianyang, 712000, Shaanxi, P.R. China

\* Corresponding Authors: [fjtes@xjtu.edu.cn](mailto:fjtes@xjtu.edu.cn) (J.T. Feng)

Fig. S1. SEM images and EDX spectra of the TiO<sub>2</sub> samples.

Fig. S2. Nitrogen adsorption-desorption isotherms (Inset are the pore size distribution) of the TiO<sub>2</sub> samples.

Fig. S3. Adsorption isotherms for ARG adsorbed onto the TiO<sub>2</sub> samples at different temperature fitting with Langmuir and Freundlich models.

Table S1. Langmuir, and Freundlich isotherm parameters for ARG adsorbed onto the TiO<sub>2</sub> samples at different temperature.



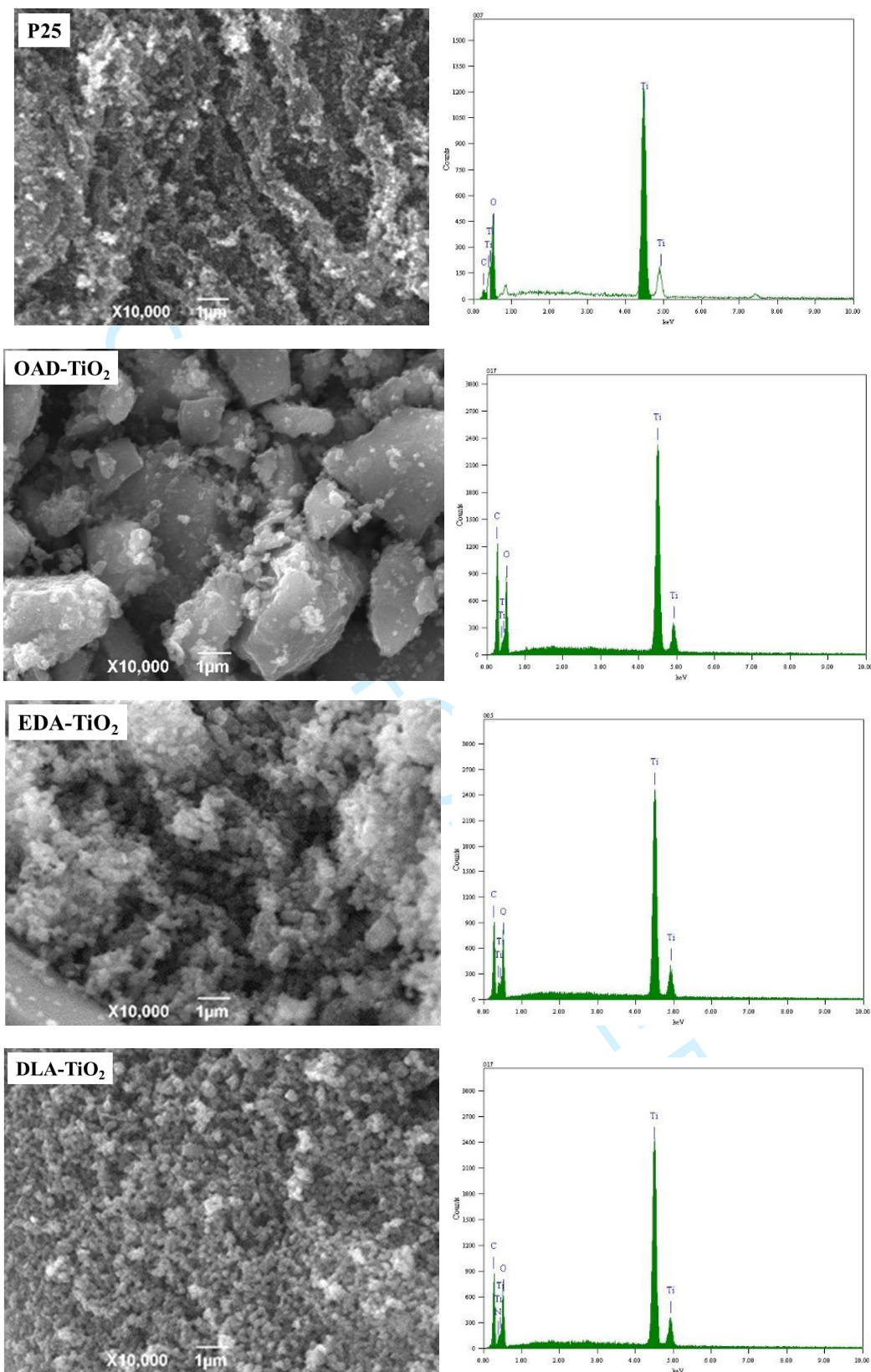
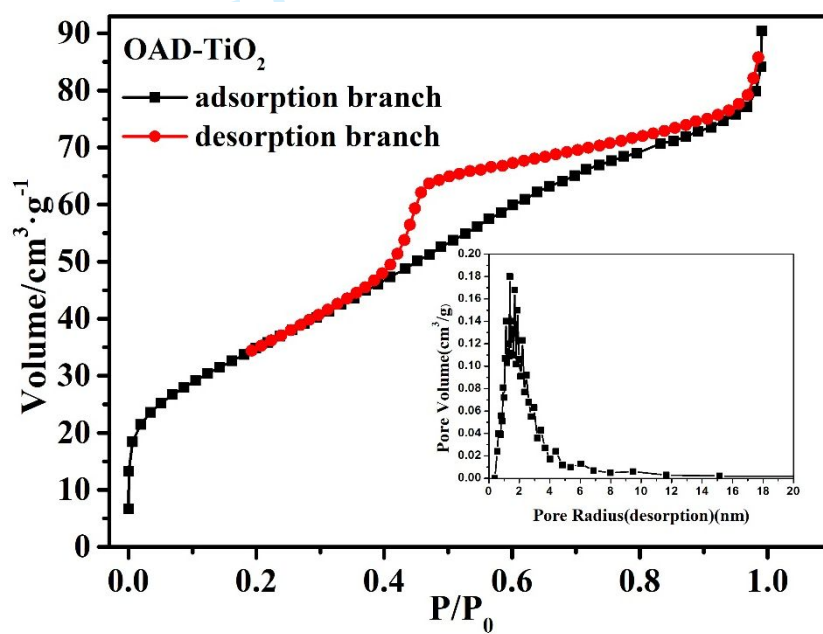
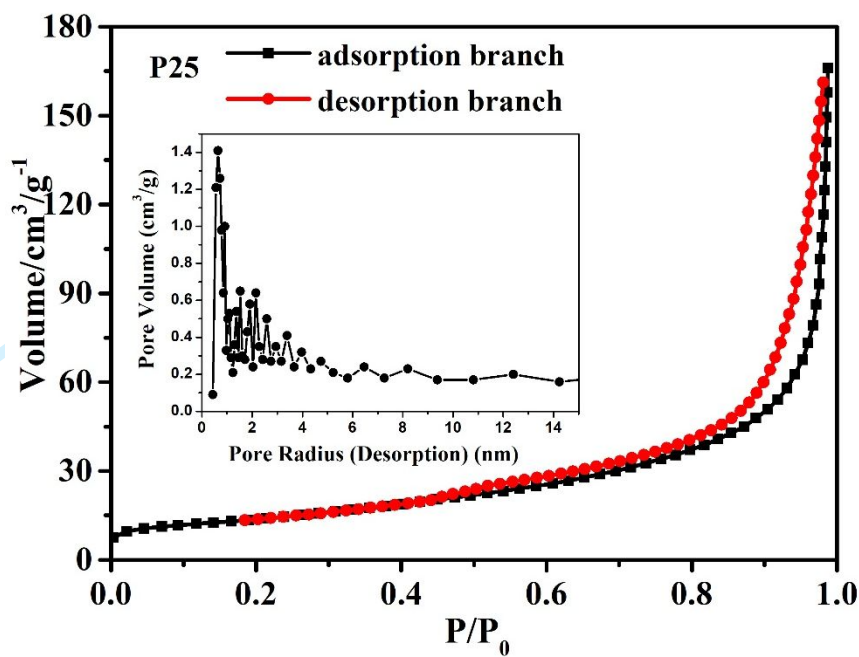


Figure S1. SEM images and EDX spectra of the TiO<sub>2</sub> samples.





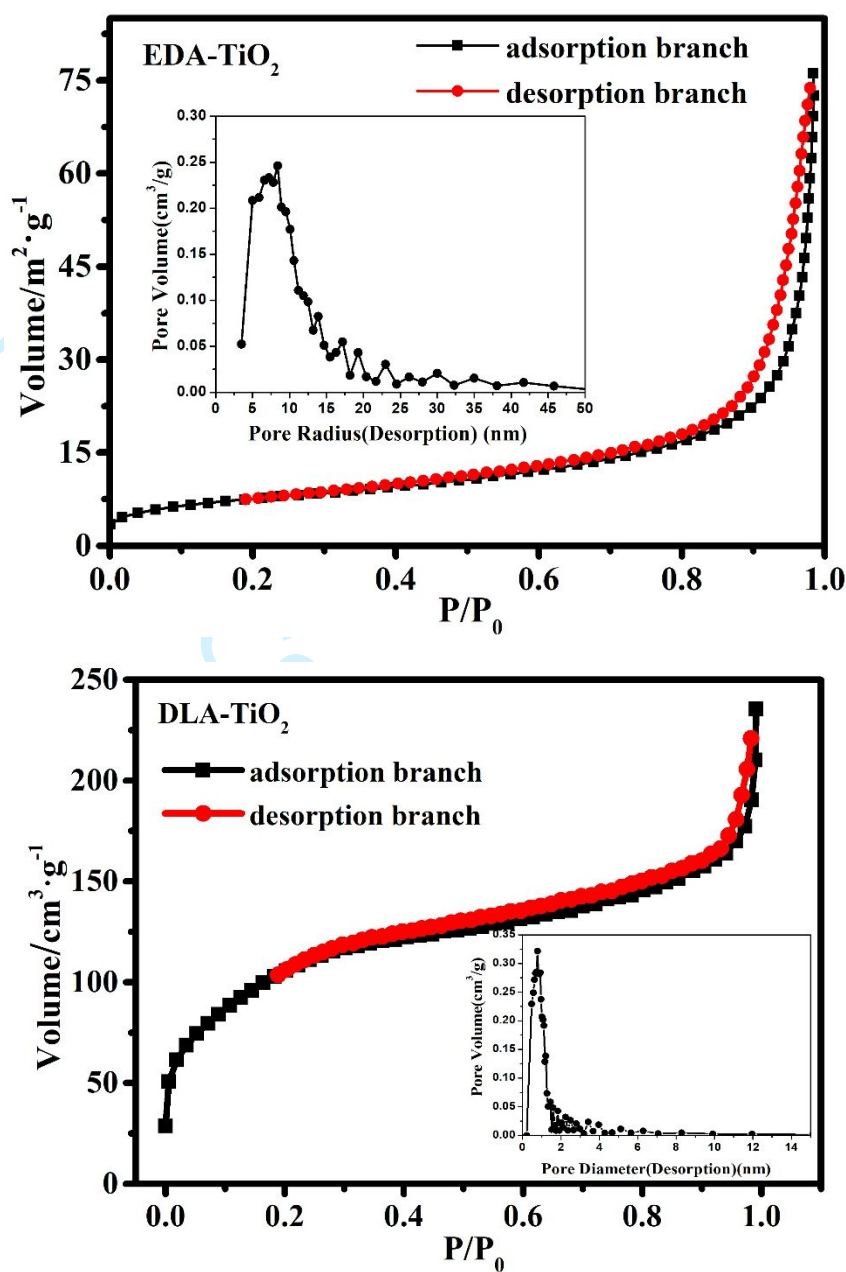
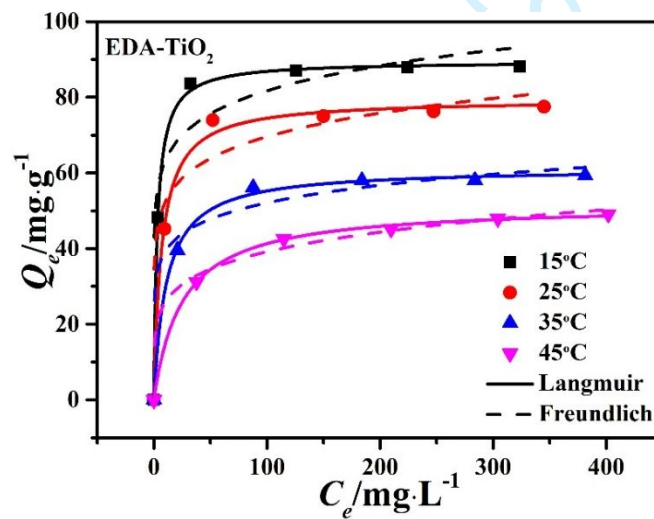
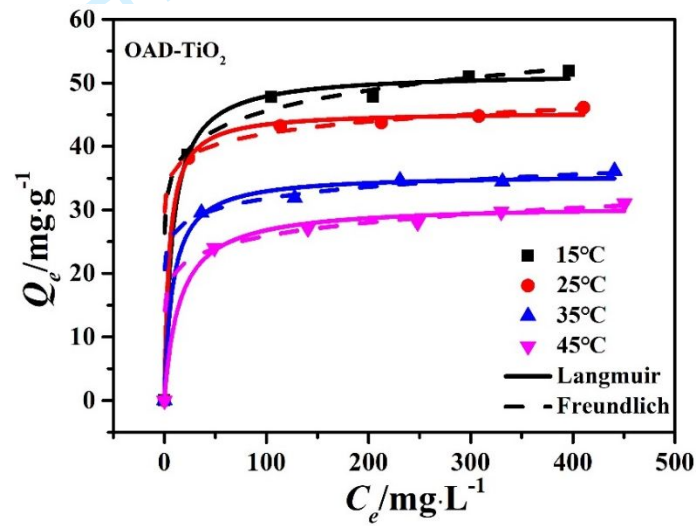
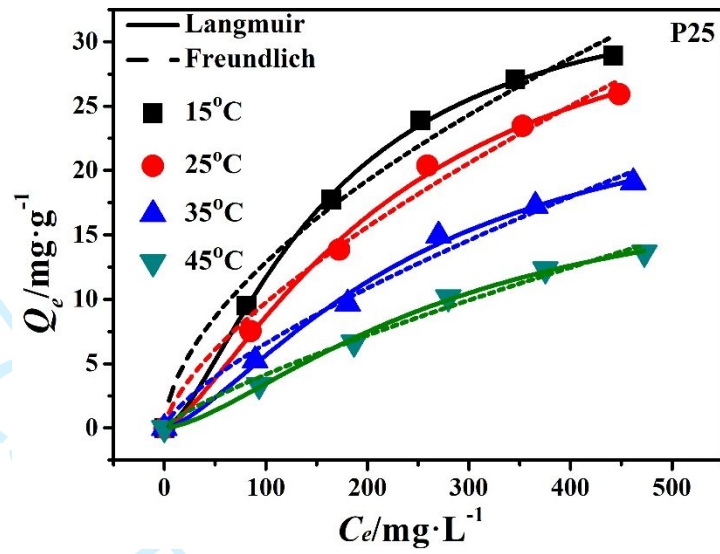


Figure S2. Nitrogen adsorption-desorption isotherms (Inset are the pore size distribution) of the TiO<sub>2</sub> samples.



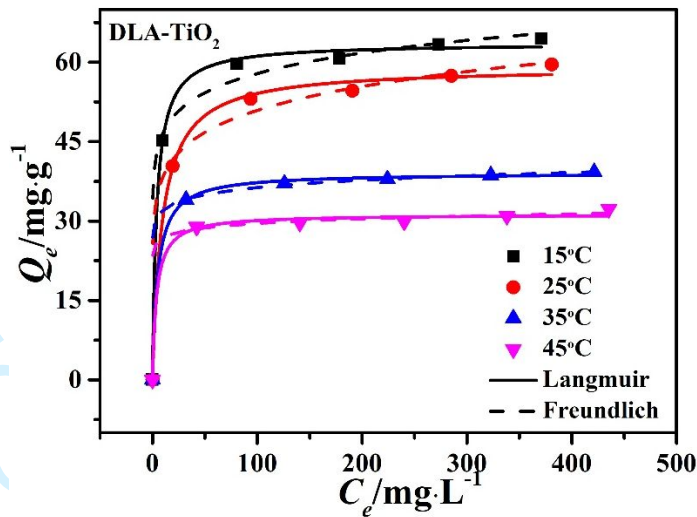


Figure S3. Adsorption isotherms for ARG adsorbed onto the TiO<sub>2</sub> samples at different temperature fitting with Langmuir and Freundlich models.

Table S1. Langmuir, and Freundlich isotherm parameters for ARG adsorbed onto the TiO<sub>2</sub> samples at different temperature.

Samples	Temp/°C	Langmuir model parameters			Freundlich model parameters		
		$Q_m(\text{mg/g})$	$K_L(\text{L/mg})$	$R^2$	$K_F((\text{mg/g})/(\text{mg/L})^n)$	$1/n$	$R^2$
P25	15	35.28	0.0049	0.9975	0.425	0.680	0.9645
	25	28.78	0.0047	0.9905	0.232	0.726	0.9611
	35	27.11	0.0032	0.9838	0.108	0.792	0.9707
	45	20.07	0.0020	0.9931	0.895	0.579	0.9456
OAD-TiO <sub>2</sub>	15	51.64	0.213	0.9963	28.96	0.10	0.9293
	25	48.11	0.128	0.9983	31.46	0.06	0.9627
	35	35.61	0.123	0.9943	22.00	0.08	0.9416
	45	30.86	0.066	0.9940	15.44	0.11	0.9722
EDA-TiO <sub>2</sub>	15	89.51	0.326	0.9991	48.85	0.11	0.7317
	25	78.15	0.148	0.9955	39.37	0.12	0.7130
	35	61.28	0.091	0.9982	29.53	0.12	0.7848
	45	51.65	0.040	0.9991	17.10	0.18	0.9320
DLA-TiO <sub>2</sub>	15	63.60	0.257	0.9975	37.64	0.09	0.9369
	25	59.07	0.250	0.9965	29.01	0.12	0.9484
	35	39.10	0.202	0.9991	28.28	0.05	0.9917
	45	31.26	0.109	0.9949	24.38	0.04	0.6866